Crystal structure, electronic structure, and thermoelectric properties of β-Zn_4Sb_3 from first principles

A. N. Qiu, L. T. Zhang,* and J. S. Wu
School of Materials Science and Engineering, Shanghai Jiao Tong University, 800 Dongchuan Road, Shanghai 200240, People's Republic of China

(Received 7 September 2009; revised manuscript received 9 December 2009; published 14 January 2010)

Due to its complex and disordered structure, the relationship between crystal structure and electronic properties of β-Zn_4Sb_3 is still ambiguous. The effect of Zn vacancy and interstitial on the structure, bonding, electronic properties, and thermoelectric properties of β-Zn_4Sb_3 has been investigated by *ab initio* calculations in this work. It is demonstrated that the Zn-Zn bond distance increases significantly whereas the Zn-Sb bond distance increases slightly after fully optimization and relaxation. This abnormality is explained by exploring the bonding properties, which may attribute to the Zn deficiency and the disordered distributions of Zn in β-Zn_4Sb_3. Our calculations show that β-Zn_4Sb_3 is a *p*-type degenerated semiconductor with an indirect gap of 0.26 eV and a direct gap of 0.33 eV. An opposite effect on the electrical conductivity and Seebeck coefficient is found for both *p*-type and *n*-type dopants. Thus doping may not be exceptionally beneficial for improving the thermoelectric properties of β-Zn_4Sb_3.

DOI: 10.1103/PhysRevB.81.035203 PACS number(s): 72.15.Jf, 61.66.Dk, 71.20.Lp, 84.60.Rb

I. INTRODUCTION

β-Zn_4Sb_3 has attracted much attention for its outstanding thermoelectric performance[1,2] between 300 and 700 K with a figure of merit $ZT=1.3$ at 670 K ($ZT=\sigma S^2T/\kappa$, where σ is the electrical conductivity, S is the Seebeck coefficient, κ is thermal conductivity, and T is the absolute temperature). This excellent performance primarily arises from its particularly low thermal conductivity (about 0.7 W m^{-1} K^{-1} at 650 K).[3] Recent studies[4,5] on the crystal structure of β-Zn_4Sb_3 revealed a considerable occupational deficiency in the main Zn site (0.89–0.92) and the occurrence of three weakly occupied interstitial Zn sites (about 0.06). It is believed that the Zn disorder in the structure and the three interstitial partially occupied Zn sites attribute to its low thermal conductivity.[6]

Although β-Zn_4Sb_3 has been identified as an excellent thermoelectric material, further improvements of thermoelectric performance are of vital importance to practical applications. Doping is an effective approach to optimize the thermoelectric properties by adjusting the carrier concentration,[7] nevertheless it is found that doping in β-Zn_4Sb_3 is not always beneficial. Liu *et al.*[8,9] and Tsutsui *et al.*[10] have investigated the effects of Al, Ga, and In doping on the thermoelectric properties of β-Zn_4Sb_3, respectively. They found that the substitutions increase both the electrical resistivity and the Seebeck coefficient resulting in a reduction in ZT at high doping levels. Pedersen *et al.*[11] have investigated the thermoelectric properties of $Hg_{0.04}Zn_{3.96}Sb_3$, which shows that the Hg doping has a minor influence on the transport properties of β-Zn_4Sb_3 and ZT remains unchanged for both the undoped and the Hg-doped samples. The effect of Mg doping has also been examined,[12] which showed that no immediate improvement of ZT was achieved.

At about 260 K,[13–15] the rhombohedral β-Zn_4Sb_3 undergoes a reversible phase transition to the monoclinic α-Zn_4Sb_3. It is surprising that the complex structure of α-Zn_4Sb_3 appears to be completely ordered with a crystallographic composition of $Zn_{13}Sb_{10}$ (2 f.u. per cell).[16,17] By inspecting the structure of Zn_4Sb_3 during the phase transition, it is found that the actual composition of β-Zn_4Sb_3 should also be $Zn_{13}Sb_{10}$ ($Zn_{3.9}Sb_3$) (Ref. 18) instead of Zn_6Sb_5 stoichiometry proposed by Mayer *et al.*[19]

Based on the Mayer's model, Kim *et al.*[20] have investigated the electronic structure of β-Zn_4Sb_3 using first-principles calculation. They found that the Fermi energy was below the valence-band edge with a band gap of about 0.4 eV. Nylén *et al.*[18] have investigated the density of states (DOS) of α-Zn_4Sb_3 ($Zn_{13}Sb_{10}$), showing a band gap of about 0.3 eV. Considering the electron fillings of the bands they predicted that β-Zn_4Sb_3 was also a narrow-gap semiconductor. By constructing complex Zn_2-Sb_2 frameworks in Zn_4Sb_3, Mikhaylushkin *et al.*[21] have concluded that the band gap of $Zn_{13}Sb_{10}$ is 0.2–0.3 eV. Cargnoni *et al.*[5] have proposed an extremely complex model with different combinations of various $Zn_{12}Sb_{10}$ and $Zn_{13}Sb_{10}$ modifications, leading β-Zn_4Sb_3 to being a *p*-type semiconductor.

Considering the disordered and interstitial Zn atoms, the relationship between crystal and electronic structures of β-Zn_4Sb_3 is still ambiguous. The effect of doping to the thermoelectric properties in experiments is also puzzling. First-principles calculations help provide a deeper understanding of the electronic structure and the physics-governing electronic transport and they are thus a powerful tool in the field of thermoelectricity. In this work, we constructed a simple virtual-crystal model with a consistent stoichiometry of β-Zn_4Sb_3 ($Zn_{13}Sb_{10}$) including a careful consideration of vacancies and interstitials. First-principles calculations were then performed to reveal the electronic structures of α-Zn_4Sb_3 and β-Zn_4Sb_3 with different crystal models. Based on the band structure and the experimental data, the thermoelectric properties of doped β-Zn_4Sb_3 were explained in detail using the Boltzmann theory and the rigid-band approach.

II. MODEL AND METHODOLOGY

The structures of α-Zn_4Sb_3 (space group $C\bar{1}$) and β-Zn_4Sb_3 of Mayer's model (space group $R\bar{3}C$) have been

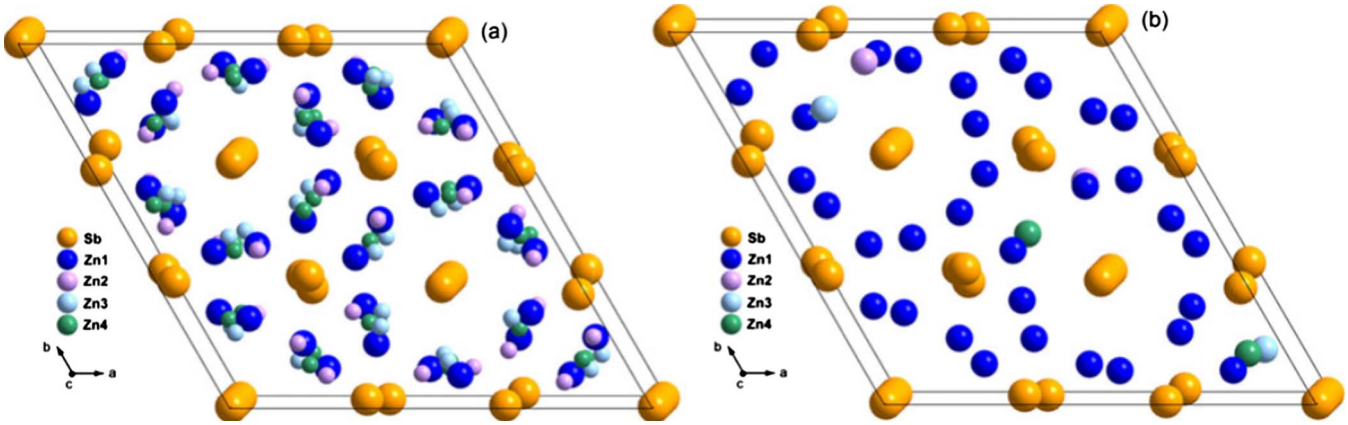

FIG. 1. (Color online) Crystal structure of (a) β-Zn_4Sb_3 in space group $R\bar{3}C$ with all atoms in full occupancy, the interstitial Zn atoms are presented in smaller spheres, (b) the $Zn_{13}Sb_{10}$ model with occupancy close to the experimental value.

proposed in detail.[18,19] According to the latest study,[4] β-Zn_4Sb_3 bears a rhombohedral crystal structure [space group $R\bar{3}C$, as shown in Fig. 1(a)]. Two nonequivalent Sb1 (18e) and Sb2 (12c) sites are fully occupied as 18 Sb^{3-} and 12 Sb^{2-} in dimers. In contrast, the main Zn1 site (36f) is only 90% partially occupied. In addition to the Zn deficiency, there are three interstitial Zn sites (36f) in the lattice with quite low occupancies (about 6%). The β-Zn_4Sb_3 cell amounts to $Zn_{13}Sb_{10}$, i.e., 39 Zn atoms and 30 Sb atoms in the unit cell.

Based on the previous comprehensive structural characterizations, the framework of β-Zn_4Sb_3 for calculations was constructed in the following way: first, a crystal was built with full occupancy of Zn1, Sb1, and Sb2 sites resulting in the $Zn_{36}Sb_{30}$ stoichiometry. Then we removed three Zn1 atoms to form three vacancies in the crystal. The distances of the vacancies were chosen to be as far as possible, which possessed the lowest total energy. Finally, we inserted different Zn interstitials couple dimers to occupy the cavity of each single Zn1 vacancy, as pointed out by Cargnoni.[5] In this way, we obtained a crystal cell [Fig. 1(b)] with a nominal composition of $Zn_{39}Sb_{30}$, which is perfectly consistent with that of β-Zn_4Sb_3. Moreover, the ratios of 0.917 (33/36) and 0.056 (2/36) are quite close to the refined occupancy of the main and interstitial Zn sites, respectively. The theoretical mass density of our model is 6.41 g/cm^3 which coincides well with the experimental value of 6.36 g/cm^3.[22]

First-principles calculation was performed by the full-potential linearized augmented plane-wave (FP-LAPW) method implanted in the WIEN2K code.[23] The exchange-correlation potentials were evaluated within the generalized gradient approximation (GGA) of Perdew, Burke, and Ernzerhof.[24] A cutoff energy of −6.5 Ry was used to separate the valence and core states. The muffin-tin radii R_{MT} was set to 2.2 a.u. for all atoms and the plane-wave cutoff constant $R_{MT}K_{max}$ was set to 7.0. The essential relaxation procedures were performed following the damped Newton dynamic schemes for forces acting on the atoms smaller than 10^{-3} Ry/a.u. Self-consistent procedure was performed on a $3\times3\times3$ k mesh in the irreducible Brillouin zone (IBZ) until the energy difference was less than 10^{-5} Ry. The thermoelectric properties were calculated from the band structure of Mayer's model using the semiclassical Boltzmann theory and the rigid-band approach.[25] For the transport tensors calculation, eigenenergies of 4218 k points on a nonshifted mesh in the IBZ were calculated by the BOLTZTRAP code,[26] which is based on a well-tested smoothed Fourier interpolation to obtain an analytical expression of the bands. The original k mesh was interpolated onto a mesh five times as dense as the original.

III. RESULTS AND DISCUSSION

A. Structural and bonding properties

The ground-state bulk properties were obtained by following the Murnaghan's[27] equation of state. Compared to the experimental value ($a=12.2282$ Å and $c=12.4067$ Å), GGA gives larger lattice constants by about 1.3% ($a=12.3933$ Å and $c=12.5742$ Å). These values are consistent with the usual GGA behavior of overestimating the unit-cell volume,[28] indicating that the accuracy of the result is satisfactory.

According to Cargnoni[5] and Mozharivskyj,[29] some of the refined distances between the main and interstitial Zn sites are quite short, which is true in our initial crystal cell (e.g., $d_{min}^{Zn2\text{-}Zn3}=1.83$ Å and $d_{min}^{Zn1\text{-}Zn4}=1.70$ Å). On the other hand, the Zn-Sb bond distances are somewhat reasonable for both Zn atoms occupying the main ($d_{min}^{Zn1\text{-}Sb1}=2.73$ Å) and interstitial ($d_{min}^{Zn4\text{-}Sb2}=2.73$ Å) sites. The short Zn-Zn bonds are unfavorable in the lattice and may induce local distortions of the lattice. This can be confirmed by our relaxation process. Table I lists the bond-length changes before and after relaxations. It is interesting to find that there is a significant change in the Zn-Zn bond distances. However, the Zn-Sb bond distances increase slightly. The minimum Zn-Zn bond distances after relaxations of local atoms increase to about 2.5 Å; compared to the 2.4 Å by Toberer.[30] A recent study[31] of the local structure of β-Zn_4Sb_3 using the pair distribution function analysis suggested the existence of nanoscale domains of locally ordered α structure which are not long-

TABLE I. Bond-length changes in Zn-Zn and Zn-Sb before and after relaxations.

	Zn_1-Zn_4	Zn_2-Zn_3	Zn_2-Zn_4	Zn_3-Zn_4	Zn_1-Sb	Zn_2-Sb	Zn_3-Sb	Zn_4-Sb
Before relaxation (Å)	2.02	1.97	2.37	2.40	2.73	2.71	2.64	2.73
After relaxation (Å)	2.53	2.52	2.58	2.63	2.78	2.75	2.79	2.77
Change ratio (%)	25.2	27.9	8.9	9.6	1.8	1.5	5.7	1.5

range ordered in the β phase. Our results show that the short Zn-Zn bonds are physically unstable and the Zn atoms seem to repulse each other to a reasonable distance in the actual local structure. This may lead to the occurrence of α-like short-range local ordering.

The above difference in changes of bond distances of Zn-Zn and Zn-Sb implies that the bonding characters between Zn-Zn and Zn-Sb may be different. To further elucidate the nature of the Zn-Zn and Zn-Sb interactions, we computed the bonding charge density, which offers an insight into the chemical bonds formed as a result of charge redistribution. The bonding charge density is defined as the difference between the total charge density in the solid and the superpositions of neutral atomic charge densities at the atom sites. Figure 2 presents the valence-bonding charge densities projected on the (110) plane of β-Zn_4Sb_3. It can be found that the bonding characteristic of β-Zn_4Sb_3 is dominantly covalent based on the directional distribution of valence electrons, which is in agreement with the results based on x-ray electron-density analysis by the maximum entropy method. Obviously, the strong and directional covalent bonds between Zn and Sb atoms are formed as the significant charge accumulations along the Zn-Sb atom pairs. In comparison, the covalent bonds between Zn and Zn atoms are rather weak. This different bonding strength explains the large increase in Zn-Zn distances and slightly changed Zn-Sb distances. In addition, the weak Zn-Zn bond may be attributed to the Zn deficiency and to the disordered distributions in β-Zn_4Sb_3 acting an important role during the phase transition from β to α at low temperatures. The weak nature of such bonding may also cause the decrease in lattice thermal conductivity (0.75 W m^{-1} K^{-1} to 0.65 W m^{-1} K^{-1} at 230 K) during the $\alpha \rightarrow \beta$ phase transition as the appearance of the disordered interstitial Zn atoms.

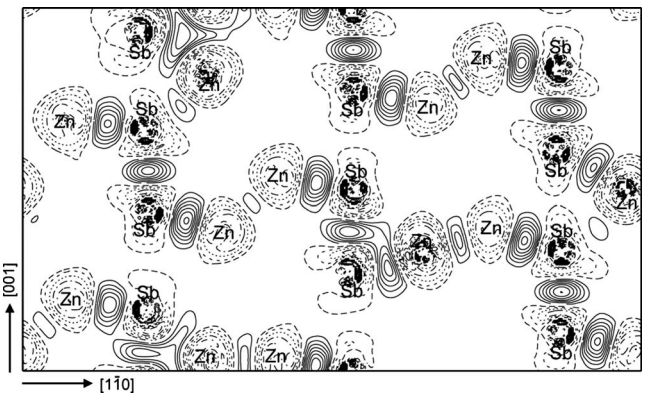

FIG. 2. Valence-bonding charge density for β-Zn_4Sb_3 on the (110) plane. Contours range from −0.2 to 0.2 e/Å^3 and increase by 0.01 e/Å^3. Solid (dotted) contours represent contours of increased (decreased) charge.

B. Electronic properties

To explore the electronic structure of β-Zn_4Sb_3, the calculated DOS is compared for the fully ordered monoclinic α-Zn_4Sb_3 ($Zn_{13}Sb_{10}$), the rhombohedral structured β-Zn_4Sb_3 proposed by Mayer ($Zn_{12}Sb_{10}$), and the interstitial β-Zn_4Sb_3 ($Zn_{13}Sb_{10}$) model (Fig. 3). For α-Zn_4Sb_3 [Fig. 3(a)], the Fermi level is exactly situated at a narrow pseudogap separating the valence and conduction bands, indicating an almost complete band filling. In Fig. 3(b) for β-Zn_4Sb_3 of Mayer's model, the Fermi level is deep inside the valence states leaving certain amount of unoccupied valence states. This may lead to a metallic behavior for β-Zn_4Sb_3, which is contrary to the narrow-gap-semiconductor behavior observed in experiments. Therefore, β-Zn_4Sb_3 should have a filled valence-bands state. Indeed, the interstitial model of β-Zn_4Sb_3 in Fig. 3(c) exhibits a narrow-gap-semiconductor character. The Fermi level is located close to the band gap and the valence states are almost filled. It is shown that the valence state extends down to about 11 eV below the Fermi level and is divided into three distinct parts [Fig. 3(d)]. The DOS of β-Zn_4Sb_3 from the bottom up to −8 eV is mainly composed of Sb *s* states. From −7.5 to −6 eV, the sharp Zn *d* states dominate the shape of DOS. From −6 eV to the Fermi level, the valence state is rather complex with mixed Zn *d*, Sb *s*, and Sb *p* hybridized states. A narrow band gap of about 0.3 eV separates the valence states to the conduction states, which is also composed of the above-mentioned hybridized states. The hybridization of conduction and valence states determines the appearance of the gap near the Fermi level. We regard these mixed hybridized states as the cause of the highly covalent bonds in β-Zn_4Sb_3.

Detailed structures of the DOS close to the Fermi energy are found to be different for the three models. The states close to the Fermi level are affected by the crystal structure as well as atomic order (models). α-Zn_4Sb_3 is a semimetal with a small pseudogap. β-Zn_4Sb_3 of Mayer model is a very strongly doped semiconductor with a large band gap while the interstitial β-Zn_4Sb_3 model is a doped semiconductor with a smaller band gap. Gao[32] and Kim[20] have found that, in order to correspond to a reported Hall concentration $n_H = 9 \times 10^{25}$ $m^{-3} = 0.1$ hole/cell in Mayer's model, the calculated Fermi level should be shifted to conduction band by about 0.025 Ry. The calculated Fermi energy of our interstitial model in Fig. 3(c) is just 0.024 Ry larger than the Fermi energy of the Mayer's model in Fig. 3(b). Thus, we believe that our interstitial model offers a highly close description of electronic structure of the disordered β-Zn_4Sb_3 in reality.

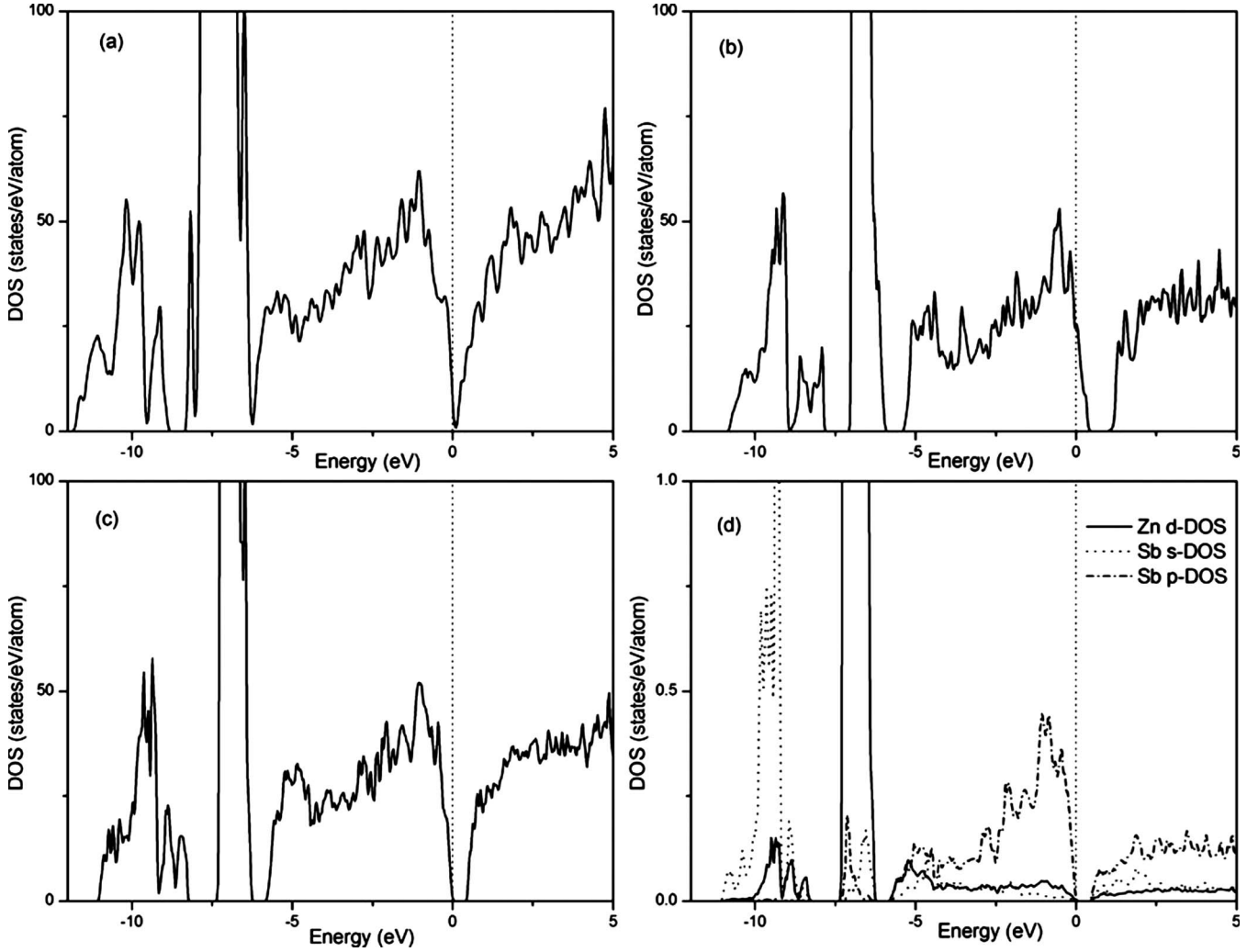

FIG. 3. The calculated total DOS of (a) α-Zn_4Sb_3, (b) β-Zn_4Sb_3 of Mayer's model, (c) β-Zn_4Sb_3, and (d) partial DOS of β-Zn_4Sb_3.

The Fermi level of β-Zn_4Sb_3 is not exactly located at the edge of band gap. The density of β-Zn_4Sb_3 at the Fermi level in the present investigation is about 0.8 states/eV/atom in Fig. 3(c). This can be illustrated more clearly in the band structure as shown in Fig. 4. The maximum valence band crosses the Fermi level, resulting in a lightly p-type degenerated semiconductor in agreement with the experiment. Only a small amount of valence band is unoccupied and induces a high carrier concentration. This clarifies the contradictory arguments of β-Zn_4Sb_3's metallic behavior by previous studies and indicates that the vacancies and interstitials in the lattice play a key role in determining its electronic structure.

The band structure in Fig. 4 reveals that β-Zn_4Sb_3 is an indirect semiconductor. The conduction-band minimum (CBM) is located at the Γ points, whereas the valence-band maximum (VBM) is located at about 4/5 of the ΓM direction. The indirect band gap is 0.26 eV and the direct gap at Γ is 0.33 eV, which both agree well with the above analysis. Our orbital composition analysis qualitatively reveals again that the VBM and CBM states are highly delocalized.

C. Thermoelectric properties

Recent studies have shown that doping in β-Zn_4Sb_3 seems unfavorable for increasing the thermoelectric properties. By exploring the band structure, the rigid-band approach can be used to investigate how thermoelectric properties depend on various doping levels.[33,34] Figure 5 presents the calculated thermoelectric properties along a and c axis of the crystal, respectively, as a function of chemical potential (i.e., versus doping level) at 600 K, without consideration of the specific dopant types. The carrier concentration as a function of chemical potential at 600 K is shown in the inset of Fig. 5(a). It is found that β-Zn_4Sb_3 shows little anisotropy in transport behaviors. The calculated Seebeck coefficient S for undoped β-Zn_4Sb_3 is 183 μV/K, which agrees well with the experimental value of 187 μV/K at 600 K (Ref. 3). By using the constant relaxation-time assumption and the experimental electrical resistivity $\rho=2.9\times10^{-5}$ Ω m, the relaxation time τ can be fitted to 3.7×10^{14} s.

Figure 5 describes an opposite influence of doping to the electrical conductivity σ and Seebeck coefficient S. For p-doped β-Zn_4Sb_3, σ increases smoothly with an increasing

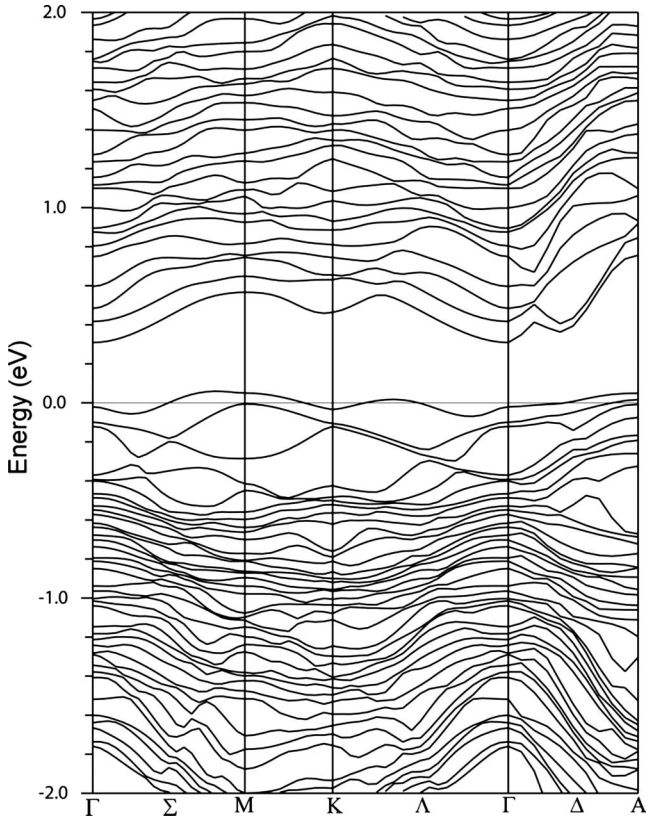

FIG. 4. The calculated band structure of β-Zn_4Sb_3.

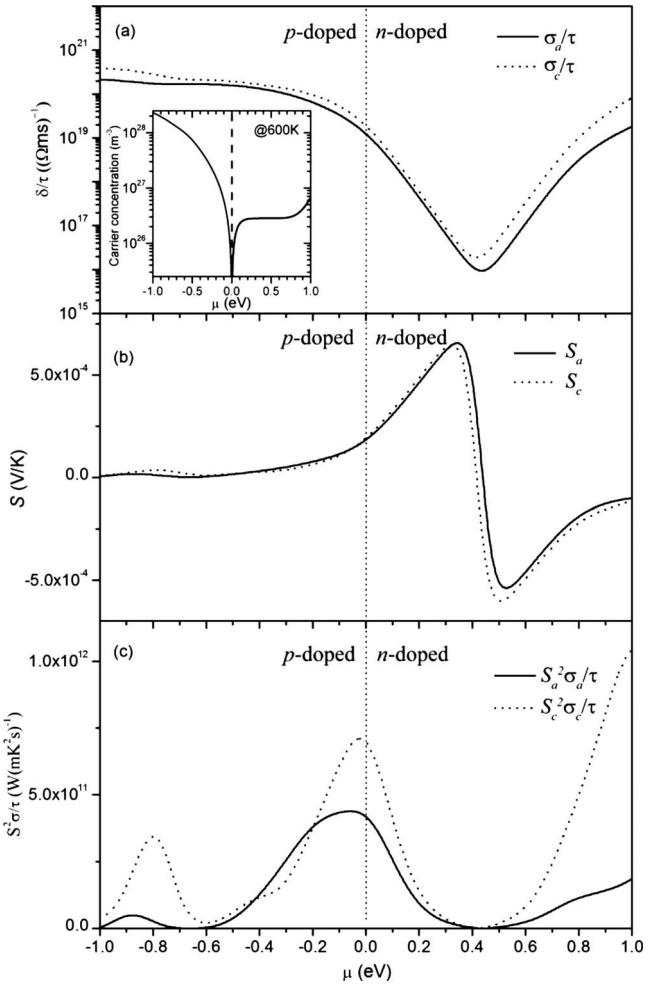

FIG. 5. The calculated thermoelectric properties along different directions of β-Zn_4Sb_3 at 600 K as a function of chemical potential. (a) Electrical conductivities relative to relaxation time σ/τ, (b) Seebeck coefficient, and (c) power factor relative to relaxation time $S^2\sigma/\tau$. The chemical potential of undoped β-Zn_4Sb_3 is marked by a vertical line at 0.0 eV. The inset shows the dependence of carrier concentration on chemical potential at 600 K.

doping amount whereas S decreases. When the chemical potential equals to −0.3 eV, the corresponding carrier concentration exceeds 10^{27} m^{-3} and S decreases to be less than 50 $\mu V/K$ [Fig. 5(b)]. For n-doped β-Zn_4Sb_3, S increases to a large value with increasing doping amount however σ decreases dramatically. Therefore the contradictory effects on S and σ result in a reduction in power factors either in p-doped or n-doped β-Zn_4Sb_3 as shown in Fig. 5(c). As a matter of fact, after doping in β-Zn_4Sb_3 (e.g., in Ref. 10), there is an increase in S the Fermi level moves toward the conduction states, thus the number of carriers at the Fermi level is decreased and the band-effective mass is increased. The combined effects of the decreased number of carriers (holes) and the increased effective mass give rise to a decreased carrier concentration and mobility, resulting in a lower σ, which is consistent with the Hall-coefficient measurement. Meanwhile, S is related to the derivatives of carrier states at the Fermi level and shows little enhancement. We note that the shape of σ and S versus doping is quite similar to those of thermoelectric materials [such as Bi_2Te_3 (Ref. 25) and $CsBi_4Te_6$ (Ref. 35)] which have optimized performance after doping, except the location of chemical potential of undoped compound. Our present calculations show that the doping is not exceptionally beneficial for raising the thermoelectric properties of β-Zn_4Sb_3. This unfavorable nature is related to its intrinsic electronic structure. Therefore, in order to improve the thermoelectric performance by doping, more attention should be paid on reducing the thermal conductivity in future experiments.

IV. CONCLUSION

In this work, we have proposed a structure model of β-Zn_4Sb_3 with the $Zn_{13}Sb_{10}$ stoichiometry close to the experimental studies, which takes the vacancies and interstitials into consideration. A first-principles calculation was performed to study its electronic properties and thermoelectric properties using the FP-LAPW method and semiclassical Boltzmann theory. Our structure-relaxation results reveal that the short Zn-Zn bonds are physically unstable and the Zn-Zn bond distances increase significantly while the Zn-Sb bond distances increase slightly. It is explained by the difference between the strong Zn-Sb covalent bonds and weak Zn-Zn covalent bonds. Our calculations show that β-Zn_4Sb_3 is a p-type semiconductor with an indirect gap of 0.26 eV and a direct gap of 0.33 eV. The valence band is not completely filled thus induces a high carrier concentration of about

9×10^{25} m^{-3}. Doping is not exceptionally beneficial for raising the thermoelectric properties. This unfavorable nature is related to the intrinsic electronic structure of β-Zn_4Sb_3 and more attention should be paid on reducing the thermal conductivity in future investigations.

ACKNOWLEDGMENTS

The authors acknowledge the financial support of the National Natural Science Foundation of China (Grant No. 50571067) and the Science and Technology Committee of Shanghai Municipal Government (Grant No. 05PJ14072).

*Corresponding author; lantingzh@sjtu.edu.cn

[1] T. Caillat, J. P. Fleurial, and A. Borshchevsky, J. Phys. Chem. Solids **58**, 1119 (1997).
[2] R. F. Service, Science **311**, 1860 (2006).
[3] M. Chitroub, F. Besse, and H. Scherrer, J. Alloy Compd. **460**, 90 (2008).
[4] G. J. Snyder, M. Christensen, E. Nishibori, T. Caillat, and B. B. Iversen, Nature Mater. **3**, 458 (2004).
[5] F. Cargnoni, E. Nishibori, P. Rabiller, L. Bertini, G. J. Snyder, M. Christensen, C. Gatti, and B. B. Iversen, Chemistry **10**, 3861 (2004).
[6] G. J. Snyder and E. S. Toberer, Nature Mater. **7**, 105 (2008).
[7] A. N. Qiu, L. T. Zhang, A. D. Shan, and J. S. Wu, Phys. Rev. B **77**, 205207 (2008).
[8] F. Liu, X. Y. Qin, and D. Li, J. Phys. D **40**, 4974 (2007).
[9] F. Liu, X. Y. Qin, and H. X. Xin, J. Phys. D **40**, 7811 (2007).
[10] M. Tsutsui, L. T. Zhang, K. Ito, and M. Yamaguchi, Intermetallics **12**, 809 (2004).
[11] B. L. Pedersen, H. Birkedal, E. Nishibori, A. Bentien, M. Sakata, M. Nygren, P. T. Frederiksen, and B. B. Iversen, Chem. Mater. **19**, 6304 (2007).
[12] B. L. Pedersen, H. Birkedal, M. Nygren, P. T. Frederiksen, and B. B. Iversen, J. Appl. Phys. **105**, 013517 (2009).
[13] S. Bhattacharya, R. P. Hermann, V. Keppens, T. M. Tritt, and G. J. Snyder, Phys. Rev. B **74**, 134108 (2006).
[14] J. Nylén, S. Lidin, M. Andersson, B. B. Iversen, H. X. Liu, N. Newman, and Ulrich Häussermann, Chem. Mater. **19**, 834 (2007).
[15] A. P. Litvinchuk, B. Lorenz, F. Chen, J. Nylén, U. Häussermann, S. Lidin, Limin Wang, and Arnold M. Guloy, Appl. Phys. Lett. **90**, 181920 (2007).
[16] Y. Mozharivskyj, A. O. Pecharsky, S. Bud'ko, and G. J. Miller, Chem. Mater. **16**, 1580 (2004).
[17] J. Nylén, S. Lidin, M. Andersson, H. Liu, N. Newman, and U. Häussermann, J. Solid State Chem. **180**, 2603 (2007).
[18] J. Nylén, M. Andersson, S. Lidin, and U. Häussermann, J. Am. Chem. Soc. **126**, 16306 (2004).
[19] H. W. Mayer, I. Mikhail, and K. Schubert, J. Less-Common Met. **59**, 43 (1978).
[20] S. G. Kim, I. I. Mazin, and D. J. Singh, Phys. Rev. B **57**, 6199 (1998).
[21] A. S. Mikhaylushkin, J. Nylén, and U. Häussermann, Chemistry **11**, 4912 (2005).
[22] V. Izard, M. C. Record, J. C. Tedenac, and S. G. Fries, CALPHAD: Comput. Coupling Phase Diagrams Thermochem. **25**, 567 (2001).
[23] K. Schwarz, P. Blaha, and G. K. H. Madsen, Comput. Phys. Commun. **147**, 71 (2002).
[24] J. P. Perdew, K. Burke, and M. Ernzerhof, Phys. Rev. Lett. **77**, 3865 (1996).
[25] T. J. Scheidemantel, C. Ambrosch-Draxl, T. Thonhauser, J. V. Badding, and J. O. Sofo, Phys. Rev. B **68**, 125210 (2003).
[26] G. K. H. Madsen and D. J. Singh, Comput. Phys. Commun. **175**, 67 (2006).
[27] F. D. Murnaghan, Proc. Natl. Acad. Sci. U.S.A. **30**, 244 (1944).
[28] I. Grinberg, N. J. Ramer, and A. M. Rappe, Phys. Rev. B **63**, 201102(R) (2001).
[29] Y. Mozharivskyj, Y. Janssen, J. L. Harringa, A. Kracher, A. O. Tsokol, and G. J. Miller, Chem. Mater. **18**, 822 (2006).
[30] E. S. Toberer, K. A. Sasaki, C. R. I. Chisholm, S. M. Haile, W. A. Goddard, and G. J. Snyder, Phys. Status Solidi (RRL) **1**, 253 (2007).
[31] H. J. Kim, E. S. Bozin, S. M. Haile, G. J. Snyder, and S. J. L. Billinge, Phys. Rev. B **75**, 134103 (2007).
[32] X. Gao, K. Uehara, D. D. Klug, S. Patchkovskii, J. S. Tse, and T. M. Tritt, Phys. Rev. B **72**, 125202 (2005).
[33] D. J. Singh and M. H. Du, Phys. Rev. Lett. **100**, 237003 (2008).
[34] G. K. H. Madsen, J. Am. Chem. Soc. **128**, 12140 (2006).
[35] L. Lykke, B. B. Iversen, and G. K. H. Madsen, Phys. Rev. B **73**, 195121 (2006).